MITSUBISHI ELECTRIC RESEARCH LABORATORIES
https://www.merl.com

Multi-Objective Motor Design Optimization with Physics-Assisted Neural Network Model

Sakamoto, Yusuke; Xu, Yihao; Wang, Bingnan; Yamamoto, Tatsuya; Nishimura, Yuki

TR2023-038 May 16, 2023

Abstract

Electric machine design optimization tasks typically require a large number of time-consuming simulations using finite-element analysis (FEA) to iteratively evaluate the design candidates. Various surrogate modeling techniques have been investigated in order to speed up the design optimization process. In recent years, machine learning based surrogate models are explored, due to their advantages including extraordinary capability in learning highly nonlinear functions. However, typical neural network based machine learning models require a large amount of training data and long training time. In this paper, we propose a multi-objective optimization (MOO) scheme for electric machine design, using a physics-assisted neural network (PANN) as surrogate model. In the PANN method, a semi-analytical subdomain physics model is used to estimate the performance of the electric machine, and this calculated result is used as the input of a neural network, in addition to other design parameters. We show that PANN can achieve the same accuracy with significantly less training data, as compared with neural networks relying solely on data. The hybrid model also shows improved accuracy with the subdomain based physics model alone. We apply the PANN surrogate model to speed up the electric machine MOO by replacing the iterative FEA based optimization process. The Pareto front solutions obtained by the proposed method are further validated with FEA with good accuracy.

IEEE International Electric Machines and Drives Conference (IEMDC) 2023

Mitsubishi Electric Research Laboratories, Inc.
201 Broadway, Cambridge, Massachusetts 02139

Multi-Objective Motor Design Optimization with Physics-Assisted Neural Network Model

Yusuke Sakamoto
Mitsubishi Electric Research Laboratories (MERL)
Cambridge, MA 02139 USA
sakamoto@merl.com

Yihao Xu
Mechanical and Industrial Engineering
Northeastern University
Boston, MA 02120 USA
xu.yiha@northeastern.edu

Bingnan Wang
Mitsubishi Electric Research Laboratories (MERL)
Cambridge, MA 02139 USA
bwang@merl.com

Tatsuya Yamamoto
Advanced Technology R&D Center
Mitsubishi Electric Corporation
Amagasaki, Hyogo 661-8661 Japan
yamamoto.tatsuya@ah.mitsubishielectric.co.jp

Yuki Nishimura
Advanced Technology R&D Center
Mitsubishi Electric Corporation
Amagasaki, Hyogo 661-8661 Japan
nishimura.yuki@dw.mitsubishielectric.co.jp

***Abstract*—Electric machine design optimization tasks typically require a large number of time-consuming simulations using finite-element analysis (FEA) to iteratively evaluate the design candidates. Various surrogate modeling techniques have been investigated in order to speed up the design optimization process. In recent years, machine learning based surrogate models are explored, due to their advantages including extraordinary capability in learning highly nonlinear functions. However, typical neural network based machine learning models require a large amount of training data and long training time. In this paper, we propose a multi-objective optimization (MOO) scheme for electric machine design, using a physics-assisted neural network (PANN) as surrogate model. In the PANN method, a semi-analytical subdomain physics model is used to estimate the performance of the electric machine, and this calculated result is used as the input of a neural network, in addition to other design parameters. We show that PANN can achieve the same accuracy with significantly less training data, as compared with neural networks relying solely on data. The hybrid model also shows improved accuracy with the subdomain based physics model alone. We apply the PANN surrogate model to speed up the electric machine MOO by replacing the iterative FEA based optimization process. The Pareto front solutions obtained by the proposed method are further validated with FEA with good accuracy.**

***Index Terms*—permanent magnet motor, design optimization, analytical model, machine learning, neural network**

I. Introduction

Motor design [1] task can often be described as multi-objective optimization (MOO) problems due to the trade-off between different design requirements. Motor design parameters are updated using heuristic optimization algorithms during the process, while each design candidate is evaluated with time-consuming numerical simulations, with finite-element method dominantly used. A large number of iterations is necessary to explore the large design space of electric machines.

Various methods have been proposed to speed up the time-consuming process. Numerous surrogate modeling techniques have been proposed and evaluated to assist the motor design optimization problem, which aim to approximate the motor performance with computationally-cheaper surrogate models. Magnetic equivalent circuit [2], polynomial response surfaces [3] and kriging method [4] are some examples of popular surrogate modeling techniques. The number of finite-element simulations required can be greatly reduced with surrogate modeling approach, and the optimization task can be completed with less time as a result. However, some of the motor performances are highly nonlinear and challenging to be estimated accurately with conventional surrogate modeling techniques. In recent years, machine learning techniques based on artificial neural networks (NNs) have found great success in various applications from computer vision to scientific computing. One of their advantages is the powerful capability in estimating highly nonlinear functions. Therefore, machine learning models have been explored for electric machine design optimization problems as well [5]–[7]. A vector of geometrical parameters or the cross-section image of a motor design is fed into the machine learning model as input, which gives prediction to desired performance metrics as output almost instantaneously. Machine learning and deep learning techniques such as convolutional neural networks (CNNs) have been applied for the prediction of various motor performances, such as torque generation [5] and nonlinear flux maps [8]–[10], and showed superior accuracy. However, one main drawback with these purely data-driven models is the large amount of training data required to achieve the desired accuracy. In practice, these data are often not readily available.

To address this problem, we propose motor design optimization scheme with a hybrid surrogate method, which combines physical model with neural network. We implement the method and apply it to the prediction of torque waveform and torque ripple of a surface-mount permanent magnet motor. The accurate estimation of the torque ripple is challenging for surrogate models, as the torque waveform is highly nonlinear and very sensitive to the slight changes in motor design

parameters. Physics-based analytical models also suffer in the accuracy of torque waveform, due to the simplifications in motor geometry and material properties needed. We show that our physics-assited neural network (PANN) model can achieve good prediction accuracy in torque ripple with a smaller training dataset as compared with purely data-driven NN, which will be called NN for simplicity in the following of the paper. The achieved accuracy also easily outperforms analytical physical models.

After establishing the surrogate model, we apply it for the multi-objective optimization of a surface-mount permanent magnet motor, aiming to maximize the average torque while minimizing the torque ripple. We show that the overall design time can be reduced compared with conventional optimization using iterative finite-element analysis (FEA). The actual performance of the obtained Pareto front designs using PANN model, as validated by FEA, also outperforms most designs obtained with purely data-driven NN surrogate model.

The rest of the paper is arranged as follows. In Section II, we describe the settings of multi-objective optimization task for a surface-mount permanent magnet motor. In Section III, we give detailed description for each step of the proposed motor design optimization work flow, including the physical model based on semi-analytical subdomain method, the proposed physics-assisted neural network model, and the multi-objective optimization process. In Section IV, we implement the proposed method, present and discuss the results, including the accuracy of the surrogate models, and the effectiveness of the multi-objective optimization process. In Section V, we conclude the paper.

II. Problem Setting

In this work, we investigate the design optimization of a surface-mounted permanent magnet (SPM) motor with 10 poles and 12 slots. A schematic drawing of the design template is shown in Fig. 1, with a total of 9 geometrical parameters subject to optimization. All other dimensions, such as the outer diameter of the stator and axial length of the motor, are fixed. The air gap between rotor and stator is fixed as $0.5\ \mathrm{mm}$. The number of winding turns and the coil current is set to be 10 turns and 15 $\mathrm{A_{rms}}$, respectively.

FEA simulations are conducted in order to construct the dataset for machine learning purposes. Firstly, design candidates are generated by randomly varying individual 9 design parameters. Then infeasible designs are removed, based on the following geometrical constraints:

$$x_5 \geq x_6. \tag{1}$$

$$(x_1 - 0.5 - x_7)\sin(\pi/10) > x_8. \tag{2}$$

The first constraint (1) works to avoid the concave shape of the tooth shoe. The second constraint (2) works to avoid overlapping of neighboring magnets. For feasible designs, magnetic simulations are conducted to calculate the generated torque at each rotor position. A total of 21 rotor angular positions are simulated over $1/6$ electric cycle for each design, and the on-load torque waveform is obtained.

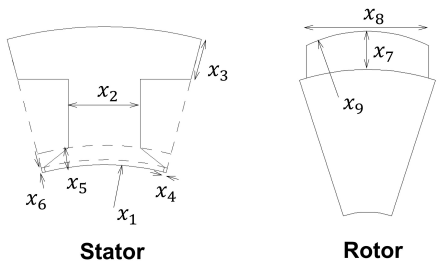

Fig. 1. A schematic for the design parameters for SPM motor

TABLE I
List of design parameters.

x_1	Rotor inner radius
x_2	Tooth width
x_3	Back yoke width
x_4	Slot opening
x_5	Tooth shoe height 1
x_6	Tooth shoe height 2
x_7	Magnet height at the center
x_8	Magnet width
x_9	Magnet curvature radius

In order to apply to neural networks, the torque waveform obtained by FEA are transformed to the Fourier series as follows:

$$\tau(\theta) = \tau_0 + \tau_1 \cos 6\theta + \tau_2 \sin 6\theta + \tau_3 \cos 12\theta + \tau_4 \sin 12\theta, \tag{3}$$

where θ is the electric angle, τ_0 is the average torque and τ_1, τ_2, τ_3, and τ_4 are the amplitude of 6th and 12th harmonics of the waveform.

Since we consider 10 poles and 12 slots SPM motor in this study, the cogging torque caused by the interaction between rotor magnets and stator slots has the 12th harmonic and its multiplier frequencies. On the other hand, at on-load condition, the torque ripple is generated by the interaction between magnet flux and coil current, and has the 6th and its multiplier harmonics. Hence, we need to pay attention to the average torque and the $6n$-th harmonics of the torque waveform. Here we focus only on the 6th and 12th harmonics, because the magnitude of the 18th and higher harmonics is relatively small and can be ignored in calculating the peak-to-peak value of torque waveform. Eventually we obtain 5 labels $\tau_0, \tau_1, \cdots, \tau_4$ and each of them is used as the output of the neural networks.

A total of 8900 motor designs are generated and simulated. After that, they are divided into 7180 training data candidates and 1720 test data. Training data are randomly picked up from the training data candidates, where the number of chosen training data is varied from 100 to 7120 in order to investigate the training data size dependence of the proposed method, as shown in the results section.

III. The Proposed Optimization Method

In this section, we first describe the semi-analytical subdomain model used to estimate the SPM motor torque waveform

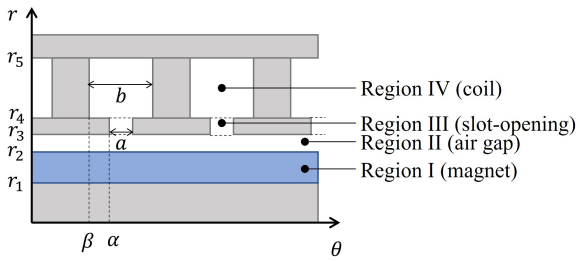

Fig. 2. The simplified subdomains of a SPM motor.

and assist the machine learning surrogate model; we then lay out the model structures for the proposed PANN model and compare it with conventional NN model; finally we formulate the MOO problem and describe the optimization process.

A. Semi-analytical subdomain model

For motor design, various analytical models have been proposed for the rapid calculation of magnetic fields and electromagnetic performances of the motor. In this work, we use a semi-analytical subdomain method based model for the torque waveform calculation of the SPM motor [11]–[15], which will be used as an initial estimate of the motor performance for the machine learning study.

The subdomain method solves for the governing equation of magnetic vector potential in the framework of magnetostatic approximation of Maxwell's equations. A few simplifications are made in order to obtain analytical solutions. First, the end effect in the axial direction is neglected and the problem is described in 2D. Then the 2D motor geometry is slightly simplified and divided into several sectors, so-called subdomain, so that each subdomain becomes a rectangular shapes in the polar (r-θ) coordinate, as shown in Fig. 2. The governing equation of the magnetic field is

$$\Delta \boldsymbol{A} = -\mu_0 \boldsymbol{J} - \mu_0 \nabla \times \boldsymbol{M}, \tag{4}$$

where $\boldsymbol{A}$, $\boldsymbol{J}$ and $\boldsymbol{M}$ is the magnetic vector potential, current density and the magnetization, respectively. $\boldsymbol{J}$ and $\boldsymbol{M}$ has non-zero value only in the coil and magnet subdomains, respectively. In the two-dimensional case, $\boldsymbol{A}$ has only one element along z direction and the general solution of (4) for each sector can be analytically derived.

For the magnet domains (Region I), the general solution is written as:

$$\begin{aligned} A_z^I(r,\theta) &= A_o^I + B_o^I \ln r \\ &+ \sum_{n=1}^{\infty} \begin{bmatrix} \left(A_n^I r^{-n} + B_n^{II} r^n + W_n(r)\right) \sin n\theta \\ + \left(C_n^I r^{-n} + D_n^I r^n - W_n(r)\right) \cos n\theta \end{bmatrix} \end{aligned} \tag{5}$$

where the integer n represents the harmonic order of the Fourier series, and W_n represents the contribution from the PM magnetization.

For the air gap (Region II), the solution is expressed as:

$$\begin{aligned} A_z^{II}(r,\theta) &= A_0^{II} + B_0^{II} \ln r \\ &+ \sum_{n=1}^{\infty} \left(A_n^{II} \left(\frac{r}{r_2}\right)^{-n} + B_n^{II} \left(\frac{r}{r_3}\right)^{n} \right) \sin n\theta \\ &+ \sum_{n=1}^{\infty} \left(C_n^{II} \left(\frac{r}{r_2}\right)^{-n} + D_n^{II} \left(\frac{r}{r_3}\right)^{n} \right) \cos n\theta \end{aligned} \tag{6}$$

where r_2 and r_3 represents the inner and outer radius of the air gap, respectively.

Similarly, for the slot-opening (Region III) and the coil (Region IV) domains, the solutions are in the following forms:

$$\begin{aligned} A_z^{III,i}(r,\theta) &= A_0^{III,i} + B_0^{III,i} \ln r \\ &+ \sum_{v=1}^{\infty} \left(A_v^{III,i} \left(\frac{r}{r_3}\right)^{-v} + B_v^{III,i} \left(\frac{r}{r_4}\right)^{v} \right) \cos[k_v^{III}(\theta - \alpha_i)] \end{aligned} \tag{7}$$

$$\begin{aligned} A_z^{IV,i}(r,\theta) &= A_0^{IV,i} + B_0^{IV,i} \ln r - \mu_0 J_z^{IV,i} r^2/4 \\ &+ \sum_{v=1}^{\infty} \left(A_v^{IV,i} \left(\frac{r}{r_4}\right)^{-v} + B_v^{IV,i} \left(\frac{r}{r_5}\right)^{v} \right) \cos[k_v^{IV}(\theta - \beta_i)] \end{aligned} \tag{8}$$

where r_3, r_4, and r_5 represents the inner and outer radius of each region (III, IV), i represents the i-th slot-opening/coil, α and β represents the starting angular position of the slot-opening and coil domains, $k_v^{III} = v\pi/a$ and $k_v^{IV} = v\pi/b$, and a and b is the angular width of the slot-opening and coil, respectively.

Magnetic flux density is computed by the rotation of the vector potential, as follows.

$$B_r = \frac{1}{r}\frac{\partial A_z}{\partial \theta}, \quad B_\theta = -\frac{\partial A_z}{\partial r}. \tag{9}$$

Coefficients in equations (5), (6), and (7) can then be determined by considering the boundary conditions. According to Maxwell's equation, the magnetic field on the boundary between subdomain i and j follows:

$$B_\perp^i = B_\perp^j, \quad H_\parallel^i = H_\parallel^j, \tag{10}$$

where $B_\perp^i$ and $B_\perp^j$ is the magnetic flux density component perpendicular to the boundary, $H_\parallel^i$ and $H_\parallel^j$ is the magnetic field component parallel to the boundary, respectively. By solving all the boundary conditions for all the set of neighboring subdomains, the magnetic vector potential in the whole calculation domain is fully determined.

The torque generted from the rotor is computed based on Maxwell's stress tensor, as

$$\tau = \frac{r_g^2 l_s}{\mu_0} \int_0^{2\pi} B_r(r_g,\theta) B_\theta(r_g,\theta) d\theta, \tag{11}$$

where r_g and l_s is the air-gap radius and the motor axial length, respectively. More details of subdomain method are described in the prior works [11]–[15].

In setting up the problem, in addition to the slight deformations of subdomains, we have also assumed that the iron permeability is infinity. That makes the boundary condition between the air and the iron much simpler, as $H_{\parallel} = 0$. However, this assumption causes error in the torque calculation because the actual permeability of the iron, in particular at the tooth shoe, can be much lower and varies with the rotational angle of the rotor, depending on the nonlinear B-H relationship of the core material. While it is in principle possible to consider finite-permeability in different core domains under the subdomain framework [15], the modeling process will unavoidably get more complicated, and iterative solvers are needed to calculate nonlinear effect; in addition, the error caused by geometrical modifications in defining the subdomains still remains. We therefore keep the infinite permeability assumption, and apply the calculation results from the subdomain method to the physics-assisted neural network model in the next step.

B. Physics-Assisted Neural Network Model

For machine learning based surrogate models, feed-forward neural networks are constructed. The surrogate modeling process is shown in Fig. 3. In a conventional NN-based surrogate model, the design parameters defined in Fig. 1 are directly treated as input to the NN, and the motor performance of our interest, namely the torque waveform Fourier coefficients $\tau_0, \tau_1, \cdots, \tau_4$ defined in (3), is output, as shown in Fig. 3 (a). The NN has an input layer, a hidden layer, and an output layer: The input layer has 9 nodes corresponding to each input parameter, the output layer has one node for one of the coefficients, and the hidden layer has 100 nodes. The Sigmoid function is used for the activation function.

In our proposed PANN model, on the other hand, as illustrated in Fig. 3 (b), the coefficient τ_k is initially estimated from the torque waveform obtained by the subdomain model described in the previous subsection, and this initial estimation is also used as input for the NN, in addition to the original design parameters. More specifically, for each motor design defined by the input parameters, the torque output is computed analytically with the subdomain model for each rotor position over a full electric cycle, the obtained time-domain torque waveform is transformed to the Fourier series as described in equation (3). The 5 desired Fourier series components calculated from the analytical model are added to the input of the PANN model for the subsequent training and testing process. As a result of this modification, the input layer dimension of the PANN model is increased from 9 to 10.

The same set of training data is used to train both NN and PANN models, and their prediction accuracies are evaluated using the same set of test data. The prediction accuracy of the trained model is evaluated by the root-mean-square error (RMSE) over the test dataset, which is defined as

$$\mathrm{RMSE}_{\mathrm{test}} = \sqrt{\frac{1}{n_{\mathrm{test}}} \sum_{i=1}^{n_{\mathrm{test}}} (y_i - \hat{y}_i)^2}, \tag{12}$$

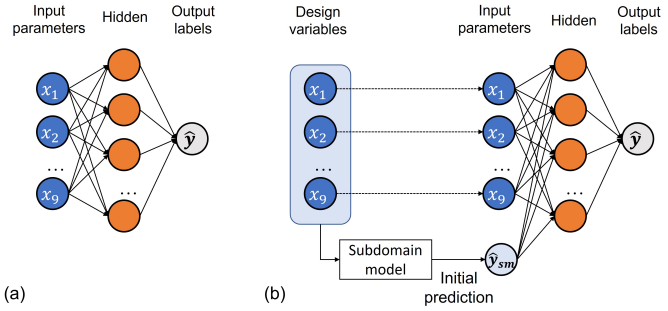

Fig. 3. The flowcharts of the process for (a) NN (b) PANN.

where n_{test} is the number of test data, $\hat{y}_i$ and y_i are the prediction of the surrogate model and the ground truth obtained by FEA for the i-th test data, respectively.

Training data of different sizes are prepared from the dataset, and used to train both NN and PANN models, in order to evaluate their performances with different training data size.

C. Multi-Objective Optimization Process

Multi-objective optimization (MOO) is then performed based on genetic algorithm (GA), where the trained surrogate models are used to estimate motor performances instead of FEA simulations for each iteration. In this study, we set two objective functions for the design optimization of SPM motor to maximize the average torque and minimize the peak-to-peak torque ripple:

$$\text{Minimize} \qquad f_1 = -\tau_0, \tag{13}$$

$$\text{Minimize} \qquad f_2 = \tau_{max} - \tau_{min}, \tag{14}$$

where τ_0 is the average torque generation over one electric cycle, τ_{max} and τ_{min} are the maximum and minimum value of the torque waveform, respectively. These two are typical and common requirements for a lot of motor applications in the industry.

Due to the trade-off between average torque and torque ripple, no single solution can be obtained to minimize both objective functions; instead, a set of Pareto solutions are obtained. NSGA-II [16] is used to perform the MOO task. The number of generations and the population size per generation is set to be 20 and 100, respectively.

To estimate the two objective functions, five NNs or five PANNs are trained individually, corresponding to the five Fourier series coefficients of the torque waveform $\tau_0, \tau_1, \cdots, \tau_4$ in (3), as shown in Fig. 4. The torque waveform is reconstructed from these coefficients, and then the objective function f_2, peak-to-peak amplitude of the torque ripple, is estimated.

For our study, both surrogate models with NN and PANN are used for the MOO task to obtain the Pareto frontier, and the actual performances of the obtained Pareto solutions are further evaluated with FEA simulations in order to evaluate the accuracy and effectiveness of the proposed optimization process.

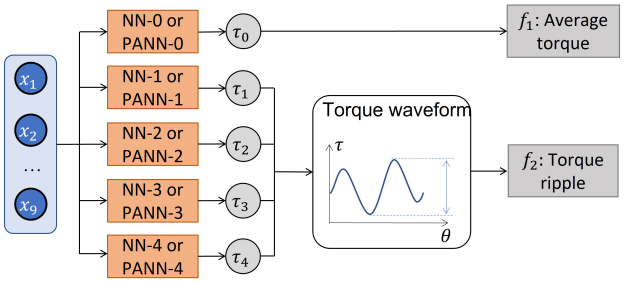

Fig. 4. The flowchart of objective function estimation using surrogate models.

IV. Results and Discussions

After establishing the design optimization workflow, we implement the method, and present the results in this section.

A. Surrogate Model Accuracy

We first train and test the accuracy of the two types of surrogate models: NN and PANN. Since the training process of machine learning models depends on the initial state of the network, 10 independent tests are carried out with the same set of training and test data, and the mean and standard deviation of the RMSE over the 10 tests are calculated.

The prediction accuracy on test data for the objective functions f_1 and f_2 with the trained surrogate models, obtained with the same training data size of 500, is shown in Fig. 5 (a) and (b), respectively, together with the result of the subdomain method based analytical model. In Fig. 5 (a) for f_1, both NN and PANN models show much smaller RMSEs than that of the subdomain model. On the other hand, in Fig. 5 (b) for f_2, the PANN model gives the smallest mean value of RMSE, as well as reduced deviation as compared with NN model.

From the results, we can see that when the physical model accuracy is low compared with purely data-driven NN prediction, it will not bring any benefits in improving the accuracy of PANN model, as in the case of Fig. 5 (a). On the other hand, when the physical model has comparable accuracy as the NN prediction, it will help improve the prediction accuracy of the proposed PANN model, as shown in Fig. 5 (b).

Fig. 5 (c) and (d) shows the relationship between training data size and prediction accuracy for the objective functions f_1 and f_2, respectively. In Fig. 5 (d), the RMSE values of f_2 with the proposed method are smaller than those of the NN when the number of training data is 500 or less and the accuracy of NN model is insufficient compared to the subdomain model. When the training data is sufficiently large (1000 or more), NN models are enough accurate and no significant difference between NN and PANN is observed. On the other hand, in Fig. 5 (c), the differences between NN and PANN are minimal for all training data sizes, since NN models have enough accuracy even with small training data. From these results, we conclude that the proposed method is especially effective when the training data is small and , and the objective function involves complicated nonlinear phenomena such as torque ripple.

B. Multi-objective Optimization

MOO tests with the three surrogate models, namely subdomain, NN and PANN, are conducted to minimize the objective functions f_1 and f_2. Both NN and PANN are trained with 500 training data, to show the ability of PANN to assist the learning process on relatively smaller dataset. Optimization results, including the Pareto solutions from the surrogate models, and their actual performances as validated by FEA, are shown in Fig. 6.

The Pareto solutions obtained by using subdomain method is shown in Fig. 6 (a). Both objective functions estimated by the surrogate model (with green $+$ markers) and validated by FEA (with green $\triangleleft$ markers) are plotted on the same graph, together with the Pareto solutions obtained by fully FEA-based GA (black dashed line), which is assumed to be the "ground truth". In this graph, the performances of the motor designs estimated by the surrogate model have relatively large discrepancies from FEA validations, and the Pareto solutions identified by the MOO with subdomain surrogate are generally worse than those obtained from FEA based MOO.

Fig. 6 (b) shows the MOO result with NN surrogate model. Compared to the case with subdomain method, the motor performances estimated by NN surrogate model are closer to the "ground truth" Pareto frontier. However, there are still large errors between surrogate estimations (with blue $\times$ markers) and FEA validations (with blue $\square$ markers) in some of obtained Pareto solutions, especially for torque ripple performances.

Fig. 6 (c) shows the Pareto solutions obtained by using the proposed PANN model. The surrogate model estimations are close to the "ground truth" Pareto frontier, as similar to the case of NN surrogate based optimization. The errors between PANN surrogate estimations (with red $+$ markers) and FEA validations (with red $\bigcirc$ markers) are much smaller than those with NN surrogate model. Direct comparison between the obtained Pareto solutions with NN and with PANN, both validated by FEA, are shown in Fig. 6 (d). It is obvious that the motor performances of almost all solutions with PANN lie close to the "ground truth" Pareto frontier, while the actual performance of some solutions obtained with NN based MOO are far from the "ground truth" Pareto frontier.

The errors between surrogate estimation and FEA validation for the obtained Pareto solutions are further quantified and summarized in Table II. For the objective function f_1, average torque, the errors of solutions obtained with both NN and PANN are in order of 10^{-2} or less, which is much smaller than that with subdomain model, and negligibe compared with the actual average torque values of Pareto solutions, which range between 2.6 and 3.1 N·m. On the other hand, for the objective function f_2, torque ripple, the accuracy of solutions obtained from PANN is significantly improved compared with that from NN, as well as subdomain model. In particular, the maximum errors of solutions from NN and subdomain model are almost 4 times larger than that of solutions from PANN. This fact implies that physics assistance can avoid large errors

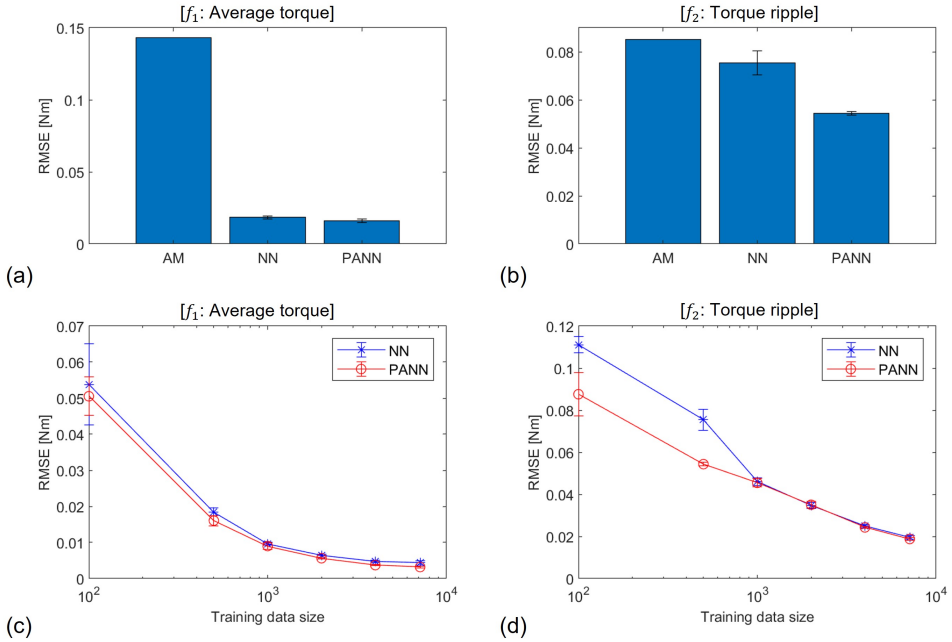

Fig. 5. The RMS errors of (a) f_1 and (b) f_2, with subdomain-bassed analytical model, and surrogate models with NN and PANN, both trained with 500 training data. RMSE of (c) f_1 and (d) f_2, as a function of training data size for the two surrogate models. Error bars show standard deviation based on 10 independent tests.

in the NN based surrogate model estimation, which leads to much improved accuracy in the Pareto frontier prediction in MOO tasks. From these results, we conclude that the proposed PANN method is most effective when the NN model and subdomain model have comparable accuracy. On the other hand, if subdomain model has insufficient accuracy, PANN model does not provide significantly accurate prediction compared with NN model.

Generally speaking, the purpose of applying data-driven surrogate models is to shorten the computational time for design optimization, while the time-consuming tasks of training data preparation is conducted before starting the optimization. The proposed method with PANN surrogate model can further reduce the data preparation time, while keeping both computational speed and prediction accuracy advantages in the design optimization process. We consider this benefit of the proposed method to be much larger if more time-consuming computations are required for the training data preparation, for example, for design tasks with 3D FEA or high-frequency iron loss calculations, or dealing with high-dimensional input parameter space where much larger dataset is needed.

V. Conclusion

In this paper, we presented a PANN surrogate model as a hybrid of physics-based analytical model and data-driven machine learning, and applied it for the multi-objective optimization of electric motors for reduced calculation time. We showed that the proposed method can achieve good accuracy for SPM motor torque ripple prediction, compared with purely data-driven NN, especially when training data size is small.

TABLE II
Comparison of Prediction Error of Pareto Solutions with NN and PANN, Validated with FEA Simulations.

	Subdomain	NN	PANN
Number of Pareto solutions	22	18	18
f_1: Average torque			
Max error [N·m]	0.596	0.028	0.016
Min error [N·m]	0.009	0.000	0.000
RMS error [N·m]	0.391	0.014	0.008
f_2: Torque ripple			
Max error [N·m]	0.150	0.165	0.040
Min error [N·m]	0.004	0.006	0.006
RMS error [N·m]	0.071	0.072	0.028

We established a MOO design process with the PANN model, which is shown to be effective in identifying motor design candidates without FEA, and accurate in predicting Pareto frontier solutions.

References

[1] G. Bramerdorfer, J. A. Tapia, J. J. Pyrhönen and A. Cavagnino, "Modern Electrical Machine Design Optimization: Techniques, Trends, and Best Practices," IEEE Trans. Ind. Electron., vol. 65, no. 10, pp. 7672-7684, 2018.

[2] C. B. Rasmussen and E. Ritchie, "A magnetic equivalent circuit approach for predicting PM motor performance," IAS '97. Conference Record of the 1997 IEEE Industry Applications Conference Thirty-Second IAS Annual Meeting, pp. 10-17 vol.1, 1997.

[3] B. H. Lee, J. P. Hong and J. H. Lee, "Optimum Design Criteria for Maximum Torque and Efficiency of a Line-Start Permanent-Magnet Motor Using Response Surface Methodology and Finite Element Method," IEEE Trans. Magn., vol. 48, no. 2, pp. 863-866, 2012.

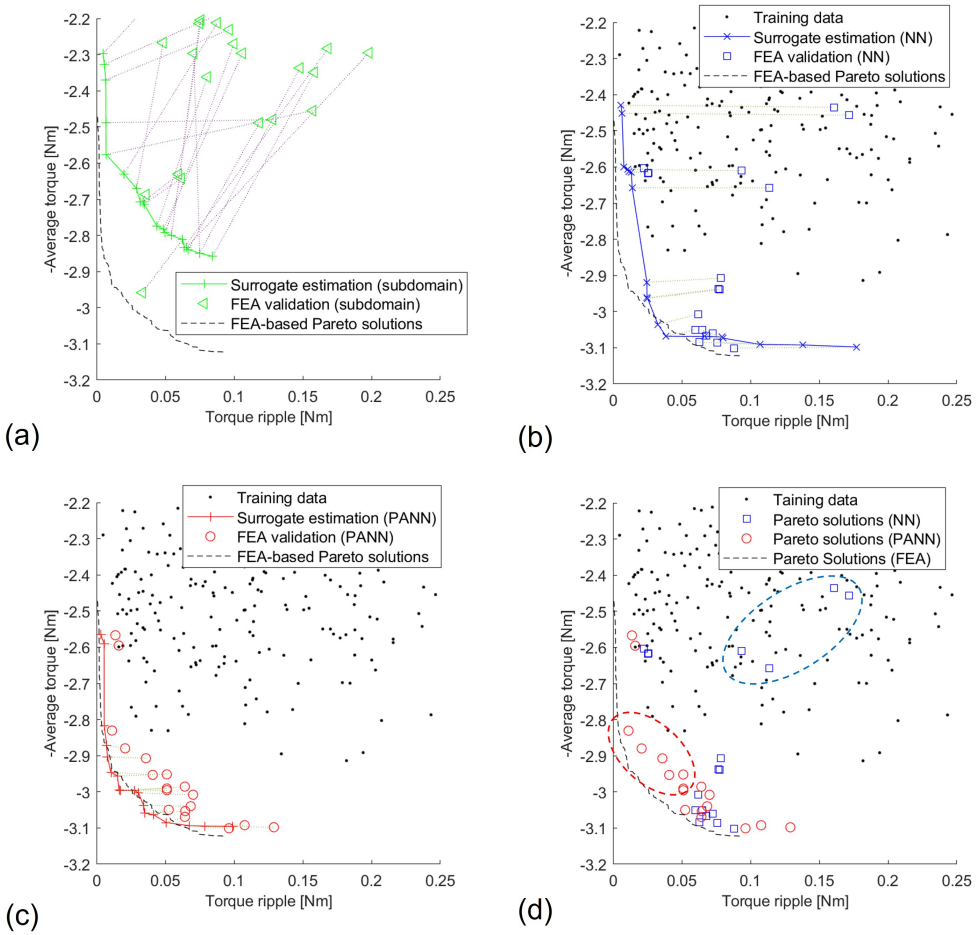

Fig. 6. The Pareto solutions of MOO obtaind by using the surrogate models. Both estimated values by each surrogate model and validated values by FEA are plotted, together with Pareto solutions obtained with FEA-based MOO: (a) subdomain, (b) NN, (c) PANN, (d) comparison of NN and PANN (FEA-validation only).

[4] M. Yousuf, F. Khan, J. Ikram, R. Badar, S. S. H. Bukhari and J. S. Ro, "Reduction of Torque Ripples in Multi-Stack Slotless Axial Flux Machine by Using Right Angled Trapezoidal Permanent Magnet," IEEE Access, vol. 9, pp. 22760-22773, 2021.

[5] L. Hadjout, N. Takorabet, R. Ibtiouen and S. Mezani, "Optimization of instantaneous torque shape of PM motors using artificial neural networks based on FE results," IEEE Trans. Magn., vol. 42, no. 4, pp. 1283-1286, 2006.

[6] T. Guillod, P. Papamanolis and J. W. Kolar, "Artificial neural network (ANN) based fast and accurate inductor modeling and design," IEEE Open J. Power Electron., vol. 1, pp. 284-299, 2020.

[7] H. Sasaki, Y. Hidaka and H. Igarashi, "Prediction of IPM machine torque characteristics using deep learning based on magnetic field distribution," IEEE Access, vol. 10, pp. 60814-60822, 2022.

[8] T. Aoyagi, Y. Otomo, H. Igarashi, H. Sasaki, Y. Hidaka and H. Arita, "Prediction of Current-Dependent Motor Torque Characteristics Using Deep Learning for Topology Optimization," IEEE Trans. Magn., vol. 58, no. 9, pp. 1-4, 2022.

[9] B. Wang, A. K. A. Talukder and Y. Sakamoto, "Topological Data Analysis for Image-based Machine Learning: Application to Electric Motors," International Conference on Electrical Machines (ICEM), pp. 1015-1021, 2022.

[10] A. K. A. Talukder, B. Wang and Y. Sakamoto, "Electric Machine Two-dimensional Flux Map Prediction with Ensemble Learning," International Conference on Electrical Machines and Systems (ICEMS), pp. 1-4, 2022. Chiang Mai, Thailand,

[11] B. L. J. Gysen, K. J. Meessen, J. J. H. Paulides and E. A. Lomonova, "General Formulation of the Electromagnetic Field Distribution in Machines and Devices Using Fourier Analysis," IEEE Trans. Magn., vol. 46, no. 1, pp. 39-52, Jan. 2010.

[12] L. J. Wu, Z. Q. Zhu, D. Staton, M. Popescu, and D. Hawkins, "Analytical prediction of electromagnetic performance of surfacemounted PM machines based on subdomain model accounting for toothtips," IET Electric Power Applications, vol. 5, pp. 597-609, 2011.

[13] S. G. Min and B. Sarlioglu, "Fast and Systematic Design Optimization of Surface-Mounted PM Machines Using Advanced Analytical Models and Subharmonic Elimination Methods," IEEE Trans. Magn., vol. 55, no. 1, pp. 1-16, 2019.

[14] B. Wang, L. Zhou, H. Wang and C. Lin, "Analytical Modeling and Design Optimization of a Vernier Permanent Magnet Motor," IEEE Energy Conversion Congress and Exposition (ECCE), pp. 4480-4485, 2021.

[15] K. Shin and B. Wang, "Semi-Analytical Modeling for Interior Permanent Magnet Synchronous Machines Considering Permeability of Rotor Core," International Conference on Electrical Machines and Systems (ICEMS), pp. 19-22, 2020.

[16] K. Deb, A. Pratap, S. Agarwal and T. Meyarivan, "A fast and elitist multiobjective genetic algorithm: NSGA-II," IEEE Trans. Evol., vol. 6, no. 2, pp. 182-197, 2002.